Self-assembled peptide dendrigraft supraparticles with potential application in pH/enzyme-triggered multistage drug release

Maximiliano L. Agazzi[1], Santiago E. Herrera[1], M. Lorena Cortez, Waldemar A. Marmisollé, Omar Azzaroni*

Instituto de Investigaciones Fisicoquímicas Teóricas y Aplicadas (INIFTA), (UNLP, CONICET), Sucursal 4, Casilla de Correo 16, 1900 La Plata, Argentina

ARTICLE INFO

ABSTRACT

Multistage delivery systems with size reduction capacity have been proposed as a powerful strategy for improving tissue drug penetration. Here we developed a simple and fast supramolecular approach to construct size-shrinkable polyamine-salt aggregates by ionic cross-linking of biodegradable poly-L-lysine dendrigraft with tripolyphosphate anion. The use of a peptide dendrimer as a nanobuilding block (~7 nm in diameter) allows the formation of supraparticles (SPs) with well-defined dimensions (~200 nm in diameter), narrow size distribution and great capacity to encapsulate different molecules, including chemotherapeutic agents as Curcumin and Doxorubicin. When exposed to slightly acidic environments, the crosslinked matrix is instantaneously disassembled to free dendrimer units. Subsequently, model cargo molecules entrapped in the dendrimer architecture can be released by the action of trypsin enzyme through peptide biodegradation. Therefore, these SPs with proved sequential pH and enzyme-responsiveness could be exploited as nanocarriers in multistage drug delivery systems.

1. Introduction

Nanotechnology and polymer science have allowed developing a wide spectrum of nanoplatforms with fascinating properties to improve anticancer chemotherapy [1,2]. Dendrimers, as the fourth new class of synthetic polymer architectures, have aroused great attention in the field of nanomedicine due to their unique three-dimensional (3D), highly branched and monodispersed structure [3,4]. Dendrigraft Poly-L-lysine (DGL) is a water-soluble peptide-based dendrimer composed only by L-lysine amino acids that - unlike traditional dendrimers, such as polyamidoamine (PAMAM) and highly branched polyethylenimine, is biodegradable, non-immunogenic, and exhibits low cytotoxicity [5–8]. Furthermore, DGLs present robust and green synthesis on a multigram scale [9]. As a consequence of their distinctive properties, DGLs have been explored in biomedical applications, including drug delivery [10–12]. However, DGLs also have several limitations to act as efficient nanocarriers: low selectivity for target cells, poor drug loading, and inadequate release profiles [13].

Another significant drawback of DGLs is associated with the small size of the dendritic nanostructures. It is well-known that particle size plays a crucial role in the accumulation/retention and penetration of nanocarriers into tumor tissues [14–17]. Because DGLs are small-sized nanoparticles (5 − 10 nm), they have a great capacity for tumor penetration but exhibit fast systemic clearance and insufficient retention in tumor environments [18,19]. Instead, larger nanoparticles (100 − 200 nm) have longer circulation times, achieving better accumulation in tumor environments but inefficient penetration due to diffusive obstacles in solid tumors [20,21]. These obstacles can be overcome with multistage drug delivery approaches based on hierarchical targeting nanoplatforms that decrease their size in response to specific tumor stimuli (including low pH and high concentrations of enzymes) [22–28].

In recent years, different strategies that involve bottom-up nanoscale engineering have been used to build responsive peptide-based dendrimer architectures with programmable size transition to improve drug penetration and therapeutic efficiency [29,30]. Gao and co-workers synthesized DGLs covalently functionalized with doxorubicin (DOX) and then linked them to the surface of gelatin nanoparticles

---

[31]. When the platform was exposed to tumor environments, the high concentration of matrix metalloproteinase-2 (MMP-2) enzymes induced the degradation of gelatin, which allowed the release of the small-sized DGL-DOX conjugates [32,33]. In another multistage approach, Cun et al. prepared nanoparticles with sequential response to enzyme/pH by conjugation of DGL with poly (ethylene glycol)-poly (caprolactone) micelles via (MMP-2)-sensitive peptide [34].

On the other hand, supramolecular chemistry offers powerful and versatile routes to create self-assembled functional supraparticles (SPs) using nanoparticles as building blocks [35–38]. Within this context, different dendritic structures have been explored as components in suprastructures with tailored properties [39–43]. Recently, supramolecular assembly of dendrimers has become a promising strategy to generate sophisticated nanocarriers with large dendritic void space and responsiveness to specific stimuli for controlled drug release [44–49].

In parallel, different cationic polyelectrolytes have been used as macromolecular building blocks to create bioinspired polyamine-salt aggregates (PSAs) [50]. Generally, these soft-materials have been formed by ionic cross-linking of linear polyamine (especially chitosan, poly(allylamine) and poly-L-lysine) with multivalent anions as polyphosphates, sulfates, citrate, succinate, among others [51–54]. PSAs have been studied as nanocarriers of drugs, genes, imaging agents and food additives due to their straightforward preparation and high loading capacity [55–58]. More importantly, since the polyelectrolyte/anion assembly is mainly induced by electrostatic interactions, PSAs have been proved to be responsive to stimuli such as pH and ionic strength changes [59–63].

Within this framework, we present a nanoarchitectonic supramolecular approach for the rational engineering of a multi-stage drug carrier based on the PSAs assembly using DGL as a 3D-polyelectrolyte building block. Therefore, we explore the self-organization of third-generation DGL into SPs by using tripolyphosphate (TPP) as anionic cross-linking agent. In this work, we show experimental evidence that confirms the formation of colloidal SPs that, under biorelevant experimental conditions, can be dismounted producing a mean size decreasing from 200 to 7 nm. Moreover, we demonstrate that after the SPs disassembly, DGLs are able to release a physically trapped cargo when exposed to trypsin, a protease overexpressed in tumor tissues [64]. Thus, electrostatically-driven cross-linking of DGL leads to the formation of dendritic polyamine-salt aggregates with improved properties to potentially act as multistage nanocarriers in pH/enzyme-triggered drug releasing systems.

2. Experimental

2.1. Chemicals

Third-generation dendrigraft poly-l-lysine (DGL, 22.0 kDa, 123 lysine residues) was provided by Colcom. Sodium tripolyphosphate (TPP), Congo Red (CR), Ethyl Orange (EO), Curcumin (CUR), Doxorubicin (DOX) and Trypsin from bovine pancreas (23.8 kDa) were purchased from Sigma-Aldrich. Sodium hydroxide and hydrochloric acid were purchased from Anedra. All chemicals were used without further purification.

2.2. DGL/TPP SPs preparation

SPs were formed by mixing equal volumes of aqueous solutions of DGL and TPP at pH = 4. Subsequently, the mixture was adjusted to pH = 7 to generate the ionically crosslinked SPs. The colloidal solution was kept at room temperature overnight to allow stabilization. After this period, no significant change in the pH of the solution was observed. DGL/TPP SPs formation was evaluated at different NH_2:TPP molar ratios (0.5 mg mL^{-1} DGL = 5 mM NH_2).

2.3. Dynamic light scattering (DLS) and zeta potential

Dynamic light scattering (DLS) and Zeta potential measurements were carried out with a ZetaSizer Nano (ZEN3600, Malvern, U.K.) at 20 °C using DTS0012 and DTS1060 disposable cuvettes, respectively. For particle size measurements, 173° backscatter angle configuration with 10 runs (10 s/run) were used for each sample. Particle Zeta potential was determined from the electrophoretic mobility by Laser Doppler Velocimetry using a general-purpose analysis method with 100 runs for each sample.

2.4. Transmission electron microscopy (TEM)

The morphology of the SPs was studied by Transmission Electron Microscopy (TEM). Samples were stained with phosphotungstic acid on carbon grids to create contrast. Images were obtained with a JEOL microscope (120 kV) equipped with a Gatan US1000 CCD camera.

2.5. Fourier transform infrared spectroscopy (FTIR)

FTIR was performed using a Varian 600 FTIR spectrometer. FTIR spectra of DGL, TPP and DGL/TPP SPs were obtained from KBr pellets.

2.6. Loading efficiency and loading capacity of SPs

The SPs loading efficiency ($\left[n_{encapsulated\ payload} / n_{total\ payload} \right] x\ 100$) was evaluated using two anionic dyes (CR and EO) and two therapeutic drugs (DOX and CUR). To incorporate each compound into the ionic networks, a payload aliquot (20 μM final concentration) was added to the DGL solutions (5 mM NH_2 final concentration prior to the SPs formation. Then, the TPP solution 0.5 mM final concentration was added to generate the loaded SPs. To evaluate the loading efficiency, the DGL/TPP/payload solution was centrifuged at 13,000 rpm for 30 min and a UV–vis spectrum of the supernatant was measured. The concentration of each compound in the supernatant was calculated using a calibration curve. The encapsulated payload moles ($n_{encapsulated\ payload}$) were calculated by subtracting the amount of compound in the supernatant from the total amount of payload ($n_{total\ payload}$) inside the microcentrifuge tubes.

The SPs loading capacity ($\left[m_{encapsulated\ payload} / m_{encapsulated\ payload} + m_{nanocarrier} \right]$ $x\ 100$) was evaluated for DOX and CUR. The incorporation of each drug within SPs was obtained following the same procedure, using a final payload concentration of 400 μM to produce the saturation of DGL molecules. The loaded SP solution 2 ml was centrifuged at 13,000 rpm for 30 min and the supernatant was discarded. Then, the pellet was dried by lyophilizing the Eppendorf tube and the total mass ($m_{encapsulated\ payload} + m_{nanocarrier}$) was obtained by weight difference between the full and empty tube. The encapsulated payload mass ($m_{encapsulated\ payload}$) was calculated indirectly measuring the target molecule concentration in the re-suspended solution by UV–vis spectroscopy against a calibration curve. UV–vis spectroscopy measurements were carried out using a Perkin Elmer Lambda 35 spectrometer. All spectra were measured between 300 and 700 nm using quartz cuvettes.

2.7. Optical transmittance measurements

The optical density of the DGL/TPP solution (5 mM NH_2/0.5 mM TPP) as a function of pH at room temperature was monitored with an Ocean Optics spectrophotometer recording the % Transmittance at 580 nm.

2.8. Triggered cargo release by trypsin

EO was used as a model drug to evaluate the release from DGL activated by trypsin. Amicon Ultra Centrifugal Filters with a molecular

weight cut-off (MWCO) of 10.0 kDa were used to separate free EO from DGL/EO complexes (DGL does not pass through the filter since it has a molecular weight higher than 10 kDa). The EO concentration trapped in the DGLs was estimated from the absorbance of the filtered solution (4500 rpm, 30 min) for the system DGL/EO (5 mM NH_2/20 μM EO) at pH = 7.0 and pH = 5.5, and for the system DGL/EO/TPP at pH = 5.5.

To evaluate EO release, a DGL/EO solution was incubated at 37 °C for three hours with trypsin (100 mg mL^{-1}) and subsequently filtered in Amicon Filters (4500 rpm, 30 min). A control experiment was performed in the same way but using denatured trypsin. For this, the enzyme was denatured by incubating in hot water (90 °C) for 1 h. The EO release extent was determined by measuring the UV–vis spectrum of the filtered solution.

3. Results and discussion

3.1. Preparation and characterization of SPs

DGL/TPP SPs were obtained by a simple one-pot one-step process in mild conditions. In order to obtain a homogeneous distribution of SPs sizes, the condensation reaction was induced by raising the solution pH to increase the charge of TPP molecules and to force the system to self-assemble. Fig. 1 shows a schematic representation of SP formation and the main interactions between DGL and TPP within the nanoparticle. As a result, a stable colloidal dispersion was obtained. It is worth mentioning that DGL was also mixed with other multivalent anions, including phosphate, sulfate, citrate, and ethylenediaminetetraacetate. However, in those cases, no formation of SPs was observed. Therefore, we focused on the study of TPP as ionic crosslinker.

The SPs self-assembly was monitored by DLS. Fig. 2a shows DLS measurements for DGL (5 mM in NH_2 residues) and DGL/TPP (5 mM NH_2/0.5 mM TPP) at pH = 7. Isolated DGL exhibited a mean hydrodynamic diameter of 7 nm, which is congruent with previously reported values [9,65,66]. In addition, DGL showed a high polydispersity index (PDI = 0.3), possibly due to the presence of aggregates formed by hydrogen bonding between DGL unimers [67]. When DGL was mixed with TPP and the solution pH adjusted to 7, SPs formation was evidenced by a significant shift in the mean hydrodynamic diameter (Fig. 2b). DGL/TPP SPs exhibit an average hydrodynamic diameter of 200 nm with a polydispersity index around 0.2. Thus, the ionic cross-linking process of DGL yields a single size distribution of colloidal SPs and a lowering in the polydispersity index compared with the analogous system without TPP. In addition, the SPs showed a Zeta potential of +27 mV, indicating that the surface exposes an excess of protonated amines. Isolated DGL presented a Zeta potential of +37 mV, evidencing that crosslinking with TPP (at a molar ratio NH_2:TPP of 1:0.1) slightly reduces the overall positive charge of the dendrimer. It is important to highlight
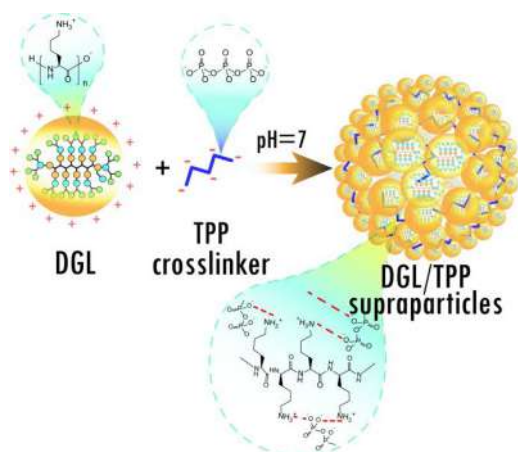

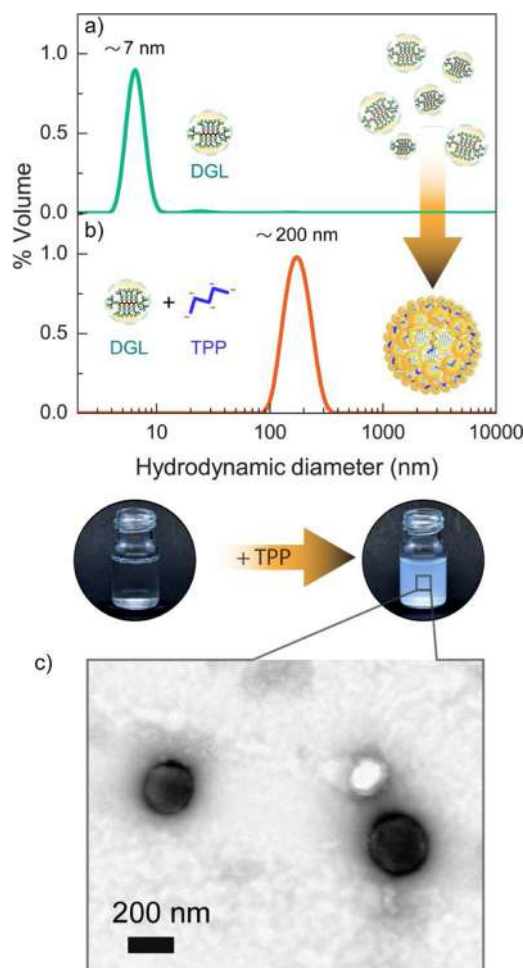**Fig. 1.** Representation of the DGL/TPP SPs self-assembly process.

Fig. 2. Hydrodynamic diameter distribution measured by DLS of (a) DGL 0.5 mg mL^{-1} and (b) DGL/TPP (5 mM NH_2/0.5 mM TPP) SPs in aqueous solution at pH = 7. (c) Transmission electron microscopy (TEM) image of DGL/TPP (5 mM NH_2/0.5 mM TPP) SPs.

that the SPs showed no tendency to aggregate or dissociate, exhibiting suitable stability within a period of 72 h (Fig. S1).

The morphology and size of DGL/TPP SPs were characterized by transmission electron microscopy (TEM). TEM image in Fig. 2c shows that SPs have a spherical structure with sizes around of 200 nm, in congruence with what was found by DLS.

Further chemical characterization of the SPs was performed by vibrational spectroscopy. Fig. 3 shows the FTIR spectra (3800 to 600 cm^{-1}) of DGL/TPP SPs and solid salts of DGL and TPP recorded in the same conditions. For DGL, the broad IR band centered around 3420 cm^{-1} can be assigned at N−H stretching vibration of free amino groups. Bands at 1650 cm^{-1} and 1540 cm^{-1} correspond to C = O stretching vibration of amide groups and N−H bending vibration, respectively [68]. The FTIR spectrum of TPP presents characteristic bands at 1218 cm^{-1} (P−O stretching), 1150 (symmetrical and asymmetric stretching vibration of the PO_2 groups), 1096 (symmetric and asymmetric stretching vibration of the PO_3 groups) and 890 cm^{-1} (P−O−P asymmetric stretching) [69,70]. In the spectrum of DGL/TPP, the peaks corresponding to DGL remain practically the same. The presence of TPP in the crosslinked matrix is confirmed by the signal at 890 cm^{-1}. The well-defined peaks at 1218, 1150 and 1096 cm^{-1} observed in the TPP spectrum disappear and, instead, a single wider signal centered at 1130 is observed. This pronounced change could be explained in terms of the complexation between DGL and TPP molecules.

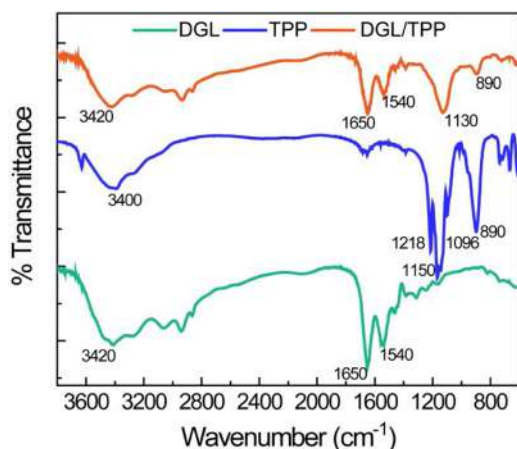SPs formation was also explored with DLS under different NH_2:TPP

Fig. 3. FTIR spectra of DGL, TPP and DGL/TPP SPs. The position of the main peaks in each spectrum is indicated in the Figure.

Table 1
Characterization of DGL/TPP SPs by DLS.

[NH_2]	[NH_2]/[TPP]	Colloidal State	d (nm)	PDI	ξ (mV)
5 mM	1:0.1	Dispersed	200	0.20	+27
5 mM	1:1	Precipitated	NA	NA	NA
0.5 mM	1:0.1	Dispersed	170	0.15	+12.7
0.5 mM	1:1	Dispersed	390	0.15	−12.5
0.5 mM	1:2	Dispersed	460	0.30	−13.2
0.5 mM	1:5	Precipitated	NA	NA	NA

d and PDI mean hydrodynamic diameter and polydispersity index, respectively.

molar ratios and concentrations of amine residues. The results are summarized in Table 1. With 5 mM NH_2 residues concentration and a 1:1 NH_2:TPP ratio, large aggregates were formed, which quickly precipitated. At a 1:0.1 ratio and a concentration ten times lower of NH_2 residues (0.5 mM), a stable colloidal suspension was observed with a hydrodynamic diameter of 170 nm and a PDI of 0.15 (Fig. S2). Furthermore, Zeta potential value decreased to a half. For higher TPP concentrations, the hydrodynamic diameter increased markedly. Thus, values of 360 nm (PDI = 0.1) and 400 nm (PDI = 0.3) were obtained for 1:1 and 1:2 ratios, respectively (Fig. S2). Interestingly, for these ratios, the Zeta potential was reversed due to the higher polyanion concentrations. This result is not trivial since in many cases the delivery systems with an excess of surface positive charges have been observed to induce cytotoxicity by interaction with cellular membranes of healthy tissues. This issue has been addressed by additional functionalization steps. In this line, functionalization with polyethylene glycol (PEG) has been reported to reduce the cytotoxicity of the DGL-based system [68,71]. In other approach, Sasaki and co-workers explored DGL as nanocarriers for gene delivery by ionic complexation with small interfering RNA (siRNA) [48]. These authors found that siRNA-DGL complexes induced cellular and hematological toxicity due to the highly cationic character ($\xi \sim$ 40 mV). To improve biocompatibility, they recharged the siRNA-DGL complexes with γ-polyglutamic acid. This biodegradable anionic compound led to the formation of ternary complexes with an excess negative charge ($\xi < 0$) yielding suitable biocompatibility. In this sense, the possibility of modulating the surface charge of the nanocarrier by varying the DGL/TPP ratio reported here may result to be a simple and direct method to improve the biocompatibility of cationic dendrimers.

Comparing the time stability for all the particles in this study, we observed that those built up from 5 mM NH_2 and 0.5 mM TPP were shown to be the most stable within 72 h post-synthesis (Fig. S1). For this reason, subsequent studies were performed with DGL/TPP (5 mM NH_2/0.5 mM TPP) SPs.
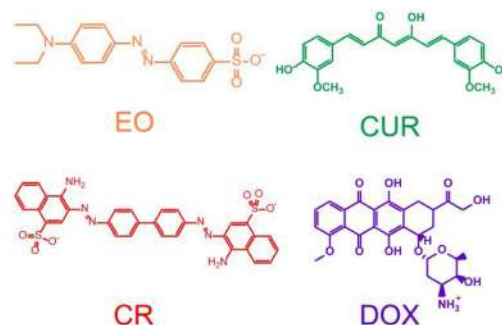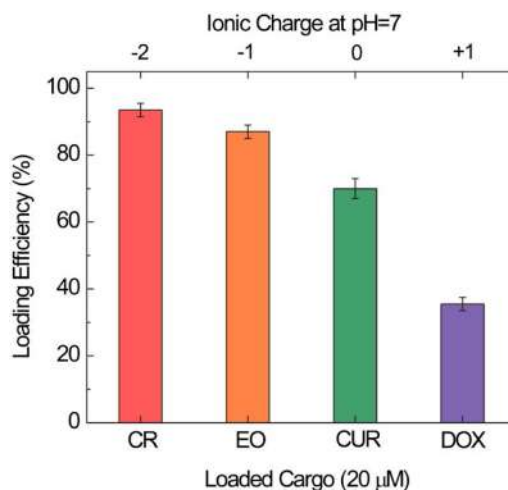

Fig. 4. DGL/TPP SPs loading efficiency of Congo Red (red), Ethyl Orange (orange), Curcumin (green) and Doxorubicin (blue) by using an initial cargo concentration of 20 μM (For interpretation of the references to colour in this figure legend, the reader is referred to the web version of this article).

3.2. Loading efficiency of SPs

The loading efficiency of DGL/TPP SPs was evaluated for four molecules with different net charges at pH = 7 (Fig. 4), by adding the cargo in the DGL solution before the assembly process with TPP. In all cases, the SPs loaded were kept at room temperature for 2 h to stabilize and the integrity of the particles was confirmed by DLS (Figs. S3b, S4b, S5b, and S6b). Two anionic dyes were used as payload models: Congo red (CR, net charge = -2) and methyl orange (EO, net charge = -1). In addition, the encapsulation of two therapeutic drugs was also evaluated: Curcumin (CUR, net charge = 0) and Doxorubicin (DOX, net charge = +1). All CR, EO, CUR and DOX UV–Vis spectra and their respective calibration curves are displayed in Supplementary Information (Figs. S3a, S4a, S5a, and S6a). To quantify the amount of each compound integrated into the SPs, the DGL/TPP/cargo solution was centrifuged and UV–vis spectrometry was performed on the supernatant.

We found almost total encapsulation when 20 μM of CR (93.5 %) and EO (87 %) were added (Fig. 4). The very high loading efficiency observed is probably due to the electrostatic interaction between anionic dyes and free protonated amines of DGL. Interestingly, SPs also showed a great capacity to encapsulate CUR (70 %), a poor water-soluble natural dye employed in a wide range of applications, including chemotherapy [72,73]. Additionally, assays were performed to assess the ability of SPs to encapsulate DOX, a broad-spectrum anti-cancer drug that presents positive net charge at pH = 7. Surprisingly, we found an encapsulation efficiency of 35.5 % for a 20 μM DOX solution, indicating that the supramolecular matrix of DGL/TPP can also encapsulate positively-charged molecules.

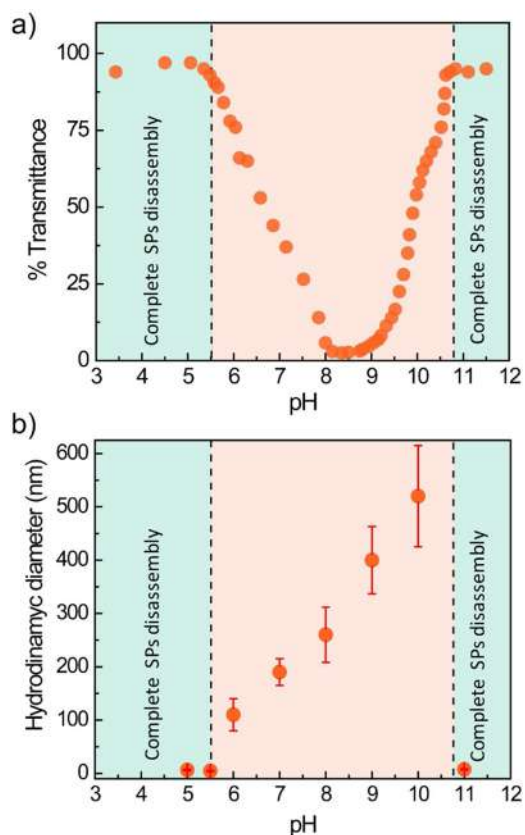In addition, the drug loading capacity of SPs was calculated for CUR

Fig. 5. Evolution of optical transmittance (a) and hydrodynamic diameter (b) of DGL/TPP SPs in aqueous solution as a function of pH.

Fig. 6. Optical transmittance and hydrodynamic diameter of DGL/TPP SPs in aqueous solution at alternating pH values (pH = 5.0 and pH = 7.4).

and DOX. We found values of 49 ± 6 % (w/w) and 18 ± 2 % (w/w) for CUR and DOX, respectively. Very recently, a CUR loading capacity of around 13 % (w/w) was found for poly-L-lysine-based nanoparticles explored as theranostic agents [74]. On the other hand, a nanoplatform based on bioreducible nanogels formed by peptide dendrimer (3 G) covalently crosslinked with disulfide bonds showed a maximum DOX loading capacity of about 17 % (w/w) [75].

3.3. pH-triggered size switching of DGL/TPP SPs

In order to explore the pH-responsive behavior of DGL/TPP SPs, the stability of the colloidal dispersions was measured at different pH conditions. For this purpose, the transmittance at 580 nm was monitored varying the pH (Fig. 5a). In addition, the hydrodynamic diameter as a function of pH was also studied (Figs. 5b and S7). The transmittance decreased when the sample was acidified as a consequence of the particles disassembly, induced by the protonation of phosphate groups in TPP [76]. Practically a total disassembly (transmittance > 90 %, green region in Fig. 5b) was found at pH around 5.5. At this pH condition, the hydrodynamic diameter corresponded to the non-crosslinked DGL, indicating a pH-triggered total transition from the SPs to the free dendrimeric state. Under alkaline conditions, a similar gradual increase in transmittance was found, observing a total dissolution of the SPs when the pH was raised over 10.5 (green region in Fig. 5a). In this condition, the disassembly is induced by the deprotonation of DGL. From pH = 7 to pH = 10, the particle size increased due to the lowering of the net positive charge of DGL (Fig. 5b), which generates a lower repulsion between the particles and facilitates their aggregation. This coagulation process was accompanied by a considerable broadening of the size distribution (Fig. S7). Additionally, the size transition driven by pH was also evaluated in physiological ionic strength (150 mM NaCl) (Fig. S8). Under these conditions, the SPs showed an
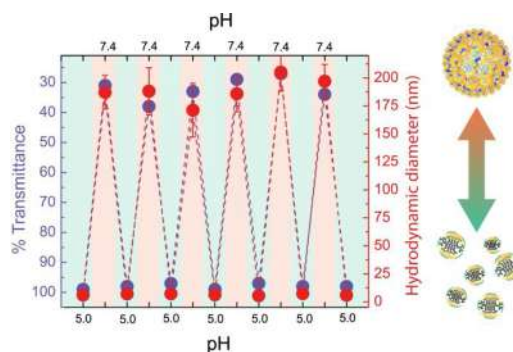
average diameter of 300 nm at pH = 7 (Fig. S8b) and have a stability window (between pH = 6 and pH = 10) narrower than in the absence of added salts (Fig. S8a). This typical behavior of the PSAs is caused by the weakening of the ionic interactions of the crosslinked network because amine groups are partially coupled to chloride anions (salt screening effects). Previously, we observed this phenomenon for the case of PSAs based on polyallylamine crosslinked with phosphate anions [54]. Thus, under acidification, size transition occurs at higher pH values, reaching a total disassembly around pH = 6.0.

To analyze the robustness and reproducibility of the size switching, we study the reversible pH-responsive assembly/disassembly of the SPs. For this, the pH of the system was successively varied between pH = 5.0 (SPs disassembly) and pH = 7.4 (SPs self-assembly). Fig. 6 shows a fully reversible behavior along consecutive formation/dissolution cycles. In this way, the system can be easily switched between two different nanoarchitectures: uniform DGL/TPP SPs (hydrodynamic diameter ∼ 200 nm) at physiological pH and isolated DGL at pH = 5 (hydrodynamic diameter ∼ 7 nm).

The pH-responsiveness of the SPs could potentially be exploited for targeted drug delivery. In this sense, it is well-known that extracellular tumor microenvironments have slightly acidic pH values (pH = 6.7–6.3) [77,78]. Furthermore, more pronounced pH gradients can be found in subcellular compartments as endosomes (pH = 5.5–6.0) and lysosomes (pH = 4.5–5.0) [79]. In addition, bacterial infections produce local acidification reaching pH values between 5.5 and 5 at the site of infection due to the production of acidic molecules (lactic acid and acetic acid) as a consequence of bacterial metabolism [80]. Considering that peptide polymers such as DGL have intrinsic antibacterial properties [11,81], DGL/TPP SPs could also be explored as pH-sensitive platforms for the treatment of infections. On the other hand, the basic pH sensibility could be considered less useful in therapeutic applications since markedly alkaline environments are not usually found in diseased tissues. However, this responsiveness could be exploited in microbial urinary infections that cause a pH increase (usually pH > 9) due to the presence of bacteria that secrete urease to catalytically hydrolyze urea into ammonia [82,83].

More interestingly, pH-triggered size transition may be useful for multistage drug delivery approaches, exploiting both the advantage of improved tumor environment accumulation properties of large-sized nanoparticles (DGL/TPP SPs) and the more efficient deep tissue penetration of small-sized nanoparticles (DGL). Following a similar approach, Wang and co-workers have developed pH-sensitive SPs (100 nm) that release small nanoparticles (5 nm) of platinum-prodrug conjugated PAMAM at the low pH of tumor environments [84,85]. Thus, the possibility of multistage disassembly is explored in the next section.

### 3.4. Triggered payload release by trypsin

So far, we have shown that DGL/TPP SPs are able to disassemble as

a response to acidic environments, releasing small-sized DGLs, which would have improved tissue penetration properties. Nevertheless, to conceptually complete the putative multistage strategy it is necessary to show that the smaller containers are able to keep the cargoes in the first disassembly step and release them in a further step, faced to a new stimulus.

Several strategies have been employed for solving this issue in multi-stage approaches based on DGL. In many of these approaches the drug was covalently linked to dendrimer by tumor stimuli-sensitive bonds, such as acid-cleavable linkages [32,34]. However, covalently linked drug systems often require synthetic processes with limited scalability and high cost. Furthermore, the therapeutic efficiency of the drug can be compromised by the chemical crosslinking. Within this context, the polypeptide biodegradation induced by proteases (over-expressed under some pathological conditions) could be rationally exploited as an alternative strategy to release physically trapped cargoes in the peptide dendritic architecture. Different reports have demonstrated that DGL is susceptible to degradation by trypsin protease [86]. In recent years, several trypsin-responsive drug delivery systems have been designed [87–90]. However, to our knowledge, there are no reports exploiting the trypsin-susceptibility of DGL to activate the controlled release.

In order to explore the trypsin-induced degradation, we incubated a DGL solution with trypsin at 37 °C and monitored the dendrimer hydrodynamic diameter as a function of time (Fig. S9). After 70 min of incubation, the peak corresponding to the DGL diameter could not be detected, indicating peptide dendrimer biodegradation induced by trypsin (Fig. S9b).

The concept of 2nd-stage cargo release was evaluated using EO as a model payload. It is worth noting that the size transition previously observed for unloaded SPs was also observed for SPs loaded with EO (Fig. S10). As the pKa of EO is 4.5, it is expected that most of the EO molecules remain negatively charged and electrostatically bound to DGL dendritic branches when the SPs are disassembled at pH 5.5. This idea was experimentally confirmed by filtration of EO/DGL solutions with Amicon Ultra Filters (Fig. S11). Fig. 7 shows that EO remains mostly trapped within the DGLs at both pH = 7 and pH = 5.5, even in the presence of TPP (column 2, 3 and 4, respectively). However, when EO-loaded DGL was exposed to trypsin (100 μg mL^{-1} at 37 °C), practically total dye release (~90 %) was observed (Column 5, Fig. 7). The enzyme-activated release was confirmed by a control experiment with denatured trypsin (Column 6, Fig. 7). In this case, a very low release was observed indicating that the EO release depends on the cleavage of DGL peptide bonds by trypsin. Thus, trypsin protease could be exploited
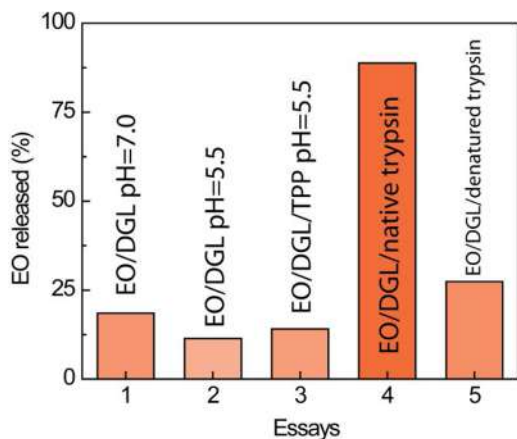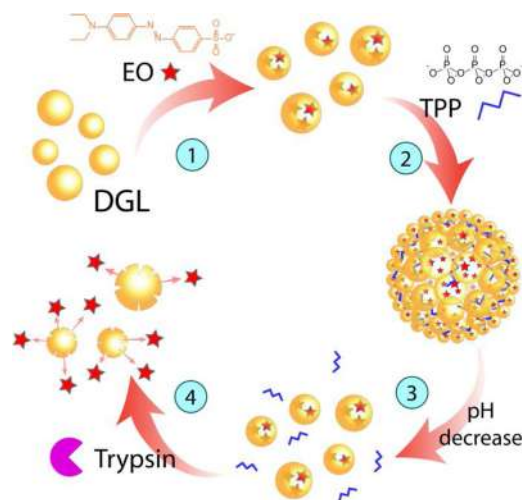
Fig. 8. Simplified representation of the potential multi-stage delivery strategy based on DGL/TPP SPs: (1) cargo encapsulation in DGL; (2) ionic-driven self-assembly of DGL to form SPs; (3) pH-triggered first disassembly stage and (4) trypsin-activated cargo release stage.

as second endogenous stimuli to site-specific drug release from the dendritic nanocontainers.

Taken together, the results obtained indicate that the dendrimeric nanoassemblies proposed here could be applied as two stage delivery carrier, exploiting firstly the acid pH sensitivity of the SPs and then, the DGL disintegration in the presence of trypsin (Fig. 8).

4. Conclusions

In this work, we expand the polyamine-salt aggregate assembly approach by using a biodegradable peptide dendrimer as a 3D-nano-building block. Applying an entirely supramolecular engineering route based on the ionic cross-linking of DGL with TPP under mild conditions, we successfully constructed pH-sensitive size-switchable dendrimer-based SPs with great ability to encapsulate different molecules. DGL/TPP suparaparticles with defined size (~200 nm-diameter) and good stability at pH = 7 were obtained. Furthermore, these SPs suffer a dramatic and sharp size transition when exposed to an acidic environment and instantaneously disassemble yielding free dendrimer building blocks (7 nm-diameter). We have also showed that an anionic model cargo is efficiently retained within the DGLs upon the SPs disassembly. Subsequently, the cargo trapped in dendritic architectures can be released by the catalytic action of an enzyme overexpressed in tumor tissues. In this way, the hierarchical integration of pH/enzyme responsiveness in the supramolecular platform can be used for promoting both deep tissue penetration and spatiotemporal controlled drug delivery.

In summary, we believe that the DGL/TPP suparaparticles discussed in this manuscript constitute promissory multistage nanocarriers with adequate properties for drug delivery applications, including the simple and straightforward preparation process, excellent loading efficiency, size reduction feature and trypsin-triggered cargo release. Further investigations in biological fluids and cellular cultures will be necessary to assess the stability, accumulation and penetration of the SPs and the individual DGLs, as previous studies for ulterior drug delivery *in vivo* applications.

Fig. 7. Percentage of the model cargo Ethyl Orange (EO) released after filtration for: 1) EO/DGL pH = 7.0, 2) EO/DGL pH = 5.5. 3) EO/DGL/TPP pH = 5.5, 4) EO/DGL/native trypsin (100 μg mL^{-1}) and 5) EO/DGL/Denatured trypsin (100 μg mL^{-1}). ([EO] = 20 μM, [NH$_2$] = 5 mM, [TPP] = 0.5 mM).

CRediT authorship contribution statement

Maximiliano L. Agazzi: Conceptualization, Data curation, Methodology, Validation, Writing - original draft, Writing - review & editing. **Santiago E. Herrera:** Conceptualization, Data curation,

Methodology, Validation, Writing - original draft, Writing - review & editing. **M. Lorena Cortez:** Conceptualization, Methodology, Writing - original draft, Writing - review & editing. **Waldemar A. Marmisollé:** Conceptualization, Writing - original draft, Writing - review & editing. **Omar Azzaroni:** Conceptualization, Writing - original draft, Writing - review & editing.

Declaration of Competing Interest

The authors declare that there are no conflicts of interest.

Acknowledgment

Appendix A. Supplementary data

Supplementary data associated with this article can be found, in the online version, at https://doi.org/10.1016/j.colsurfb.2020.110895.

References

[1] D. Peer, J.M. Karp, S. Hong, O.C. Farokhzad, R. Margalit, R. Langer, Nanocarriers as an emerging platform for cancer therapy, Nat. Nanotechnol. 2 (2007) 751–760.
[2] X. Tang, W.S. Loc, C. Dong, G.L. Matters, P.J. Butler, M. Kester, C. Meyers, Y. Jiang, J.H. Adair, The use of nanoparticulates to treat breast cancer, Nanomedicine 12 (2017) 2367–2388.
[3] S. Svenson, The dendrimer paradox – high medical expectations but poor clinical translation, Chem. Soc. Rev. 44 (2015) 4131–4144.
[4] S. Mignani, S. El Kazzouli, M. Bousmina, J.-P. Majoral, Dendrimer space concept for innovative nanomedicine: a futuristic vision for medicinal chemistry, Prog. Polym. Sci. 38 (2013) 993–1008.
[5] J. Chamieh, J.P. Biron, L. Cipelletti, H. Cottet, Monitoring biopolymer degradation by Taylor dispersion analysis, Biomacromolecules 16 (2015) 3945–3951.
[6] B. Romestand, J.-L. Rolland, A. Commeyras, G. Coussot, I. Desvignes, R. Pascal, O. Vandenabeele-Trambouze, Dendrigraft poly-l-lysine: a non-immunogenic synthetic carrier for antibody production, Biomacromolecules 11 (2010) 1169–1173.
[7] M. Tang, H. Dong, Y. Li, T. Ren, Harnessing PEG-cleavable strategy to balance cytotoxicity, intracellular release and therapeutic effect of dendrigraft poly-L-lysine for cancer gene therapy, J. Mater. Chem. B 4 (2016) 1284–1295.
[8] Y. Liu, S. An, J. Li, Y. Kuang, X. He, Y. Guo, H. Ma, Y. Zhang, B. Ji, C. Jiang, Brain-targeted co-delivery of therapeutic gene and peptide by multifunctional nanoparticles in Alzheimer's disease mice, Biomaterials 80 (2016) 33–45.
[9] H. Collet, E. Souaid, H. Cottet, A. Deratani, L. Boiteau, G. Dessalces, J.-C. Rossi, A. Commeyras, R. Pascal, An expeditious multigram-scale synthesis of Lysine Dendrigraft (DGL) polymers by aqueous N -carboxyanhydride polycondensation, Chem. - A Eur. J. 16 (2010) 2309–2316.
[10] C. Shi, Y. He, X. Feng, D. Fu, ε-Polylysine and next-generation dendrigraft poly-L-lysine: chemistry, activity, and applications in biopharmaceuticals, J. Biomater. Sci. Polym. Ed. 26 (2015) 1343–1356.
[11] J.-P. Francoia, L. Vial, Everything you always wanted to know about poly-l-lysine dendrigrafts (but were afraid to ask), Chem. - A Eur. J. 24 (2018) 2806–2814.
[12] K.T. Al-Jamal, W.T. Al-Jamal, J.T.-W. Wang, N. Rubio, J. Buddle, D. Gathercole, M. Zloh, K. Kostarelos, Cationic poly-l-lysine dendrimer complexes doxorubicin and delays tumor growth in vitro and in vivo, ACS Nano 7 (2013) 1905–1917.
[13] J. Bugno, H. Hsu, S. Hong, Tweaking dendrimers and dendritic nanoparticles for controlled nano-bio interactions: potential nanocarriers for improved cancer targeting, J. Drug Target 23 (2015) 642–650.
[14] C. He, Y. Hu, L. Yin, C. Tang, C. Yin, Effects of particle size and surface charge on cellular uptake and biodistribution of polymeric nanoparticles, Biomaterials 31 (2010) 3657–3666.
[15] A. Albanese, P.S. Tang, W.C.W. Chan, The effect of nanoparticle size, shape, and surface chemistry on biological systems, Annu. Rev. Biomed. Eng. 14 (2012) 1–16.
[16] J. Mosquera, I. García, L.M. Liz-Marzán, Cellular uptake of nanoparticles versus small molecules: a matter of size, Acc. Chem. Res. 51 (2018) 2305–2313.
[17] E. Vlashi, L.E. Kelderhouse, J.E. Sturgis, P.S. Low, Effect of folate-targeted nanoparticle size on their rates of penetration into solid tumors, ACS Nano 7 (2013) 8573–8582.
[18] S.D. Perrault, C. Walkey, T. Jennings, H.C. Fischer, W.C.W. Chan, Mediating tumor targeting efficiency of nanoparticles through design, Nano Lett. 9 (2009) 1909–1915.
[19] H. Cabral, Y. Matsumoto, K. Mizuno, Q. Chen, M. Murakami, M. Kimura, Y. Terada, M.R. Kano, K. Miyazono, M. Uesaka, N. Nishiyama, K. Kataoka, Accumulation of sub-100 nm polymeric micelles in poorly permeable tumours depends on size, Nat. Nanotechnol. 6 (2011) 815–823.
[20] J. Li, W. Ke, H. Li, Z. Zha, Y. Han, Z. Ge, Endogenous stimuli-sensitive multistage polymeric micelleplex anticancer drug delivery system for efficient tumor penetration and cellular internalization, Adv. Healthc. Mater. 4 (2015) 2206–2219.
[21] S. Ruan, W. Xiao, C. Hu, H. Zhang, J. Rao, S. Wang, X. Wang, Q. He, H. Gao, Ligand-mediated and enzyme-directed precise targeting and retention for the enhanced treatment of glioblastoma, ACS Appl. Mater. Interfaces 9 (2017) 20348–20360.
[22] C. Ju, R. Mo, J. Xue, L. Zhang, Z. Zhao, L. Xue, Q. Ping, C. Zhang, Sequential intra-intercellular nanoparticle delivery system for deep tumor penetration, Angew. Chemie Int. Ed. 53 (2014) 6253–6258.
[23] C. Wong, T. Stylianopoulos, J. Cui, J. Martin, V.P. Chauhan, W. Jiang, Z. Popovic, R.K. Jain, M.G. Bawendi, D. Fukumura, Multistage nanoparticle delivery system for deep penetration into tumor tissue, Proc. Natl. Acad. Sci. 108 (2011) 2426–2431.
[24] S. Wang, P. Huang, X. Chen, Hierarchical targeting strategy for enhanced tumor tissue accumulation/retention and cellular internalization, Adv. Mater. 28 (2016) 7340–7364.
[25] S. Cao, L.K.E.A. Abdelmohsen, J. Shao, J. van den Dikkenberg, E. Mastrobattista, D.S. Williams, J.C.M. van Hest, pH-induced transformation of biodegradable multilamellar nanovectors for enhanced tumor penetration, ACS Macro Lett. 7 (2018) 1394–1399.
[26] S. Ruan, X. Cao, X. Cun, G. Hu, Y. Zhou, Y. Zhang, L. Lu, Q. He, H. Gao, Matrix metalloproteinase-sensitive size-shrinkable nanoparticles for deep tumor penetration and pH triggered doxorubicin release, Biomaterials 60 (2015) 100–110.
[27] Y. Niu, J. Zhu, Y. Li, H. Shi, Y. Gong, R. Li, Q. Huo, T. Ma, Y. Liu, Size shrinkable drug delivery nanosystems and priming the tumor microenvironment for deep intratumoral penetration of nanoparticles, J. Control. Release 277 (2018) 35–47.
[28] G. Nagel, A. Sousa-Herves, S. Wedepohl, M. Calderón, Matrix metalloproteinase-sensitive multistage nanogels promote drug transport in 3D tumor model, Theranostics 10 (2020) 91–108.
[29] X. Cai, H. Zhu, Y. Zhang, Z. Gu, Highly efficient and safe delivery of VEGF siRNA by bioreducible fluorinated peptide dendrimers for cancer therapy, ACS Appl. Mater. Interfaces 9 (2017) 9402–9415.
[30] X. Cai, R. Jin, J. Wang, D. Yue, Q. Jiang, Y. Wu, Z. Gu, Bioreducible fluorinated peptide dendrimers capable of circumventing various physiological barriers for highly efficient and safe gene delivery, ACS Appl. Mater. Interfaces 8 (2016) 5821–5832.
[31] G. Hu, Y. Wang, Q. He, H. Gao, Multistage drug delivery system based on microenvironment-responsive dendrimer–gelatin nanoparticles for deep tumor penetration, RSC Adv. 5 (2015) 85933–85937.
[32] G. Hu, X. Chun, Y. Wang, Q. He, H. Gao, Peptide mediated active targeting and intelligent particle size reduction-mediated enhanced penetrating of fabricated nanoparticles for triple-negative breast cancer treatment, Oncotarget 6 (2015) 41258–41274.
[33] G. Hu, H. Zhang, L. Zhang, S. Ruan, Q. He, H. Gao, Integrin-mediated active tumor targeting and tumor microenvironment response dendrimer-gelatin nanoparticles for drug delivery and tumor treatment, Int. J. Pharm. 496 (2015) 1057–1068.
[34] X. Cun, M. Li, S. Wang, Y. Wang, J. Wang, Z. Lu, R. Yang, X. Tang, Z. Zhang, Q. He, A size switchable nanoplatform for targeting the tumor microenvironment and deep tumor penetration, Nanoscale 10 (2018) 9935–9948.
[35] Y. Xia, T.D. Nguyen, M. Yang, B. Lee, A. Santos, P. Podsiadlo, Z. Tang, S.C. Glotzer, N.A. Kotov, Self-assembly of self-limiting monodisperse supraparticles from polydisperse nanoparticles, Nat. Nanotechnol. 6 (2011) 580–587.
[36] T. Wang, D. LaMontagne, J. Lynch, J. Zhuang, Y.C. Cao, Colloidal superparticles from nanoparticle assembly, Chem. Soc. Rev. 42 (2013) 2804–2823.
[37] E. Piccinini, D. Pallarola, F. Battaglini, O. Azzaroni, Self-limited self-assembly of nanoparticles into supraparticles: towards supramolecular colloidal materials by design, Mol. Syst. Des. Eng. 1 (2016) 155–162.
[38] S. Wintzheimer, T. Granath, M. Oppmann, T. Kister, T. Thai, T. Kraus, N. Vogel, K. Mandel, Supraparticles: functionality from uniform structural motifs, ACS Nano 12 (2018) 5093–5120.
[39] B.N.S. Thota, L.H. Urner, R. Haag, Supramolecular architectures of dendritic amphiphiles in water, Chem. Rev. 116 (2016) 2079–2102.
[40] H. Wang, S. Wang, H. Su, K.-J. Chen, A.L. Armijo, W.-Y. Lin, Y. Wang, J. Sun, K. Kamei, J. Czernin, C.G. Radu, H.-R. Tseng, A supramolecular approach for preparation of size-controlled nanoparticles, Angew. Chemie Int. Ed. 48 (2009) 4344–4348.
[41] C. Stoffelen, J. Voskuhl, P. Jonkheijm, J. Huskens, Dual stimuli-responsive self-assembled supramolecular nanoparticles, Angew. Chemie Int. Ed. 53 (2014) 3400–3404.
[42] C. Stoffelen, J. Huskens, Size-tunable supramolecular nanoparticles mediated by ternary cucurbit[8]uril host–guest interactions, Chem. Commun. 49 (2013) 6740–6742.
[43] H. Sun, L. Miao, J. Li, S. Fu, G. An, C. Si, Z. Dong, Q. Luo, S. Yu, J. Xu, J. Liu, Self-assembly of cricoid proteins induced by "Soft nanoparticles": an approach to design multienzyme-cooperative antioxidative systems, ACS Nano 9 (2015) 5461–5469.
[44] Y. Kodama, T. Nakamura, T. Kurosaki, K. Egashira, T. Mine, H. Nakagawa, T. Muro, T. Kitahara, N. Higuchi, H. Sasaki, Biodegradable nanoparticles composed of dendrigraft poly-l-lysine for gene delivery, Eur. J. Pharm. Biopharm. 87 (2014) 472–479.

[45] X. Xu, Y. Jian, Y. Li, X. Zhang, Z. Tu, Z. Gu, Bio-inspired supramolecular hybrid dendrimers self-assembled from low-generation peptide dendrons for highly efficient gene delivery and biological tracking, ACS Nano 8 (2014) 9255–9264.

[46] Y. Li, Y. Li, X. Zhang, X. Xu, Z. Zhang, C. Hu, Y. He, Z. Gu, Supramolecular PEGylated dendritic systems as pH/redox dual-responsive theranostic nanoplatforms for platinum drug delivery and NIR imaging, Theranostics 6 (2016) 1293–1305.

[47] Y. Li, X. Xu, X. Zhang, Y. Li, Z. Zhang, Z. Gu, Tumor-specific multiple stimuli-activated dendrimeric nanoassemblies with metabolic blockade surmount chemotherapy resistance, ACS Nano 11 (2017) 416–429.

[48] Y. Kodama, H. Kuramoto, Y. Mieda, T. Muro, H. Nakagawa, T. Kurosaki, M. Sakaguchi, T. Nakamura, T. Kitahara, H. Sasaki, Application of biodegradable dendrigraft Poly-l-lysine to a small interfering RNA delivery system, J. Drug Target 25 (2017) 49–57.

[49] Y. Li, Y. Lai, X. Xu, X. Zhang, Y. Wu, C. Hu, Z. Gu, MS, Capsid-like supramolecular dendritic systems as pH-responsive nanocarriers for drug penetration and site-specific delivery, Nanomed. Nanotechnol. Biol. Med. 12 (2016) 355–364.

[50] H.G. Bagaria, M.S. Wong, Polyamine-salt aggregate assembly of capsules as responsive drug delivery vehicles, J. Mater. Chem. 21 (2011) 9454–9466.

[51] R.K. Rana, V.S. Murthy, J. Yu, M.S. Wong, Nanoparticle self-assembly of hierarchically ordered microcapsule structures, Adv. Mater. 17 (2005) 1145–1150.

[52] V.S. Murthy, R.K. Rana, M.S. Wong, Nanoparticle-assembled capsule synthesis: formation of colloidal polyamine-salt intermediates, J. Phys. Chem. B 110 (2006) 25619–25627.

[53] Y. Lapitsky, Ionically crosslinked polyelectrolyte nanocarriers: recent advances and open problems, Curr. Opin. Colloid Interface Sci. 19 (2014) 122–130.

[54] S.E. Herrera, M.L. Agazzi, M.L. Cortez, W.A. Marmisollé, M. Tagliazucchi, O. Azzaroni, Polyamine colloids cross-linked with phosphate ions: towards understanding the solution phase behavior, ChemPhysChem 20 (2019) 1044–1053.

[55] B. Hu, C. Pan, Y. Sun, Z. Hou, H. Ye, B. Hu, X. Zeng, Optimization of fabrication parameters to produce chitosan−tripolyphosphate nanoparticles for delivery of tea catechins, J. Agric. Food Chem. 56 (2008) 7451–7458.

[56] N. Zhao, H.G. Bagaria, M.S. Wong, Y. Zu, A nanocomplex that is both tumor cell-selective and cancer gene-specific for anaplastic large cell lymphoma, J. Nanobiotechnology 9 (2011) 2.

[57] A. Farashishiko, S.E. Plush, K.B. Maier, A. Dean Sherry, M. Woods, Crosslinked shells for nano-assembled capsules: a new encapsulation method for smaller Gd 3 + -loaded capsules with exceedingly high relaxivities, Chem. Commun. 53 (2017) 6355–6358.

[58] V.S. Murthy, M.S. Wong, Enzyme Encapsulation Using Nanoparticle-Assembled Capsules, (2008), pp. 214–232.

[59] H. Zhang, S. Mardyani, W.C.W. Chan, E. Kumacheva, Design of biocompatible chitosan microgels for targeted pH-Mediated intracellular release of ccancer therapeutics, Biomacromolecules 7 (2006) 1568–1572.

[60] P.G. Lawrence, Y. Lapitsky, Ionically cross-linked poly(allylamine) as a stimulus-responsive underwater adhesive: ionic strength and pH effects, Langmuir 31 (2015) 1564–1574.

[61] W.A. Marmisollé, J. Irigoyen, D. Gregurec, S. Moya, O. Azzaroni, Supramolecular surface chemistry: substrate-independent, phosphate-driven growth of polyamine-based multifunctional thin films, Adv. Funct. Mater. 25 (2015) 4144–4152.

[62] M.L. Agazzi, S.E. Herrera, M.L. Cortez, W.A. Marmisollé, C. von Bilderling, L.I. Pietrasanta, O. Azzaroni, Continuous assembly of supramolecular polyamine–phosphate networks on surfaces: preparation and permeability properties of nanofilms, Soft Matter 15 (2019) 1640–1650.

[63] S.E. Herrera, M.L. Agazzi, M.L. Cortez, W.A. Marmisollé, C. Bilderling, O. Azzaroni, Layer-by-layer formation of polyamine-salt aggregate/polyelectrolyte multilayers. Loading and controlled release of probe molecules from self-assembled supramolecular networks, Macromol. Chem. Phys. (2019) 1900094.

[64] B. Law, C. Tung, Proteolysis: a biological process adapted in drug delivery, therapy, and imaging, Bioconjugate Chem. 20 (2009) 1683–1695.

[65] N. Yevlampieva, A. Dobrodumov, O. Nazarova, O. Okatova, H. Cottet, Hydrodynamic behavior of dendrigraft polylysines in water and dimethylformamide, Polymers (Basel) 4 (2012) 20–31.

[66] J.-C. Rossi, B. Maret, K. Vidot, J.-P. Francoia, M. Cangiotti, S. Lucchi, C. Coppola, M.F. Ottaviani, Multi-technique characterization of Poly-L-lysine Dendrigrafts-Cu (II) complexes for biocatalysis, Macromol. Biosci. 15 (2015) 275–290.

[67] H. Cottet, M. Martin, A. Papillaud, E. Souaïd, H. Collet, A. Commeyras, Determination of dendrigraft poly-l-Lysine diffusion coefficients by taylor

[68] X.-X. Li, J. Chen, J.-M. Shen, R. Zhuang, S.-Q. Zhang, Z.-Y. Zhu, J.-B. Ma, pH-Sensitive nanoparticles as smart carriers for selective intracellular drug delivery to tumor, Int. J. Pharm. 545 (2018) 274–285.

[69] S. Rodrigues, A.M.R. da Costa, A. Grenha, Chitosan/carrageenan nanoparticles: effect of cross-linking with tripolyphosphate and charge ratios, Carbohydr. Polym. 89 (2012) 282–289.

[70] M. Gierszewska, J. Ostrowska-Czubenko, Chitosan-based membranes with different ionic crosslinking density for pharmaceutical and industrial applications, Carbohydr. Polym. 153 (2016) 501–511.

[71] R. Huang, S. Liu, K. Shao, L. Han, W. Ke, Y. Liu, J. Li, S. Huang, C. Jiang, Evaluation and mechanism studies of PEGylated dendrigraft poly-L-lysines as novel gene delivery vectors, Nanotechnology 21 (2010) 265101.

[72] S. Shishodia, M.M. Chaturvedi, B.B. Aggarwal, Role of curcumin in cancer therapy, Curr. Probl. Cancer 31 (2007) 243–305.

[73] A. Goel, S. Jhurani, B.B. Aggarwal, Multi-targeted therapy by curcumin: how spicy is it? Mol. Nutr. Food Res. 52 (2008) 1010–1030.

[74] D.H. Yang, H.J. Kim, K. Park, J.K. Kim, H.J. Chun, Preparation of poly-l-lysine-based nanoparticles with pH-sensitive release of curcumin for targeted imaging and therapy of liver cancer in vitro and in vivo, Drug Deliv. 25 (2018) 950–960.

[75] D. Zhong, Z. Tu, X. Zhang, Y. Li, X. Xu, Z. Gu, Bioreducible peptide-dendrimeric nanogels with abundant expanded voids for efficient drug entrapment and delivery, Biomacromolecules 18 (2017) 3498–3505.

[76] M. Gierszewska, J. Ostrowska-Czubenko, Equilibrium swelling study of crosslinked chitosan membranes in water, buffer and salt solutions, Prog. Chem. Appl. Chitin Deriv. 21 (2016) 55–62.

[77] D. Schmaljohann, Thermo- and pH-responsive polymers in drug delivery, Adv. Drug Deliv. Rev. 58 (2006) 1655–1670.

[78] W. Wu, L. Luo, Y. Wang, Q. Wu, H.-B. Dai, J.-S. Li, C. Durkan, N. Wang, G.-X. Wang, Endogenous pH-responsive nanoparticles with programmable size changes for targeted tumor therapy and imaging applications, Theranostics 8 (2018) 3038–3058.

[79] M. Kanamala, W.R. Wilson, M. Yang, B.D. Palmer, Z. Wu, Mechanisms and biomaterials in pH-responsive tumour targeted drug delivery: a review, Biomaterials 85 (2016) 152–167.

[80] T. Wei, Q. Yu, H. Chen, Responsive and synergistic antibacterial coatings: fighting against bacteria in a smart and effective way, Adv. Healthc. Mater. 8 (2019) 1801381.

[81] F. Oukacine, B. Romestand, D.M. Goodall, G. Massiera, L. Garrelly, H. Cottet, Study of antibacterial activity by capillary electrophoresis using multiple UV detection points, Anal. Chem. 84 (2012) 3302–3310.

[82] N.J. Irwin, C.P. McCoy, D.S. Jones, S.P. Gorman, Infection-responsive drug delivery from urinary biomaterials controlled by a novel kinetic and thermodynamic approach, Pharm. Res. 30 (2013) 857–865.

[83] C.P. McCoy, N.J. Irwin, C. Brady, D.S. Jones, L. Carson, G.P. Andrews, S.P. Gorman, An infection-responsive approach to reduce bacterial adhesion in urinary biomaterials, Mol. Pharm. 13 (2016) 2817–2822.

[84] H.-J. Li, J.-Z. Du, X.-J. Du, C.-F. Xu, C.-Y. Sun, H.-X. Wang, Z.-T. Cao, X.-Z. Yang, Y.-H. Zhu, S. Nie, J. Wang, Stimuli-responsive clustered nanoparticles for improved tumor penetration and therapeutic efficacy, Proc. Natl. Acad. Sci. 113 (2016) 4164–4169.

[85] H.-J. Li, J.-Z. Du, J. Liu, X.-J. Du, S. Shen, Y.-H. Zhu, X. Wang, X. Ye, S. Nie, J. Wang, Smart superstructures with ultrahigh pH-sensitivity for targeting acidic tumor microenvironment: instantaneous size switching and improved tumor penetration, ACS Nano 10 (2016) 6753–6761.

[86] G. Coussot, Y. Ladner, C. Bayart, C. Faye, V. Vigier, C. Perrin, On-line capillary electrophoresis-based enzymatic methodology for the study of polymer-drug conjugates, J. Chromatogr. A 1376 (2015) 159–166.

[87] K. Radhakrishnan, A.M. Raichur, Biologically triggered exploding protein based microcapsules for drug delivery, Chem. Commun. 48 (2012) 2307–2309.

[88] K. Radhakrishnan, J. Tripathy, A.M. Raichur, Dual enzyme responsive microcapsules simulating an "OR" logic gate for biologically triggered drug delivery applications, Chem. Commun. 49 (2013) 5390–5392.

[89] K. Wang, D.-S. Guo, M.-Y. Zhao, Y. Liu, A supramolecular vesicle based on the complexation of p -Sulfonatocalixarene with protamine and its trypsin-triggered controllable-release properties, Chem. - A Eur. J. 22 (2016) 1475–1483.

[90] X.-F. Hou, Y. Chen, Y. Liu, Enzyme-responsive protein/polysaccharide supramolecular nanoparticles, Soft Matter 11 (2015) 2488–2493.

dispersion analysis, Biomacromolecules 8 (2007) 3235–3243.